Proofreading-deficient coronaviruses adapt over long-term passage for increased fidelity and fitness without reversion of exoribonuclease-inactivating mutations

Kevin W. Graepel,[a,b,c] Xiaotao Lu,[b,c] James Brett Case,[a,b,c] Nicole R. Sexton,[a,b,c] Everett Clinton Smith,[b,c,d]# Mark R. Denison,[a,b,c]#

Departments of Pathology, Microbiology and Immunology[a] and Pediatrics[b], and Elizabeth B. Lamb Center for Pediatric Research[c], Vanderbilt University Medical Center, Nashville, Tennessee, USA; Department of Biology, The University of the South, Sewanee, Tennessee, USA[d]

Running Head: Adaptation of proofreading-deficient coronaviruses

#Address correspondence to Mark Denison, mark.denison@vanderbilt.edu, or Clint Smith, ecsmith@sewanee.edu

Abstract word count: 219

Text word count: 5,739

ABSTRACT

The coronavirus (CoV) RNA genome is the largest among single-stranded positive sense RNA viruses. CoVs encode a proofreading 3′→5′exoribonuclease within nonstructural protein 14 (nsp14-ExoN) that is responsible for CoV high-fidelity replication. Alanine substitution of ExoN catalytic residues [ExoN(-)] in SARS-CoV and murine hepatitis virus (MHV) disrupts ExoN activity, yielding viable mutant viruses with defective replication, up to 20-fold decreased fidelity, and increased susceptibility to nucleoside analogs. To test the stability of the ExoN(-) genotype and phenotype, we passaged MHV-ExoN(-) 250 times in cultured cells (P250), in parallel with WT-MHV. Compared to MHV-ExoN(-) P3, MHV-ExoN(-) P250 demonstrated enhanced replication, reduced susceptibility to nucleoside analogs, and increased competitive fitness. However, passage did not select for complete or partial reversion at the ExoN-inactivating mutations. We identified novel amino acid changes within the RNA-dependent RNA polymerase (nsp12-RdRp) and nsp14 of MHV-ExoN(-) P250 that partially account for the observed changes in replication, susceptibility to nucleoside analogs, and competitive fitness observed in the passaged virus population, indicating that additional determinants can compensate for the activities of nsp14-ExoN. Our results suggest that while selection favors restoration of replication fidelity in ExoN(-) CoVs, there may be a significant barrier to ExoN(-) reversion. These results also support the hypothesis that high-fidelity replication is linked to CoV fitness and identify additional candidate proteins that may regulate CoV replication fidelity.

IMPORTANCE

Unique among RNA viruses, CoVs encode a proofreading exoribonuclease (ExoN) in nsp14 that mediates high-fidelity RNA genome replication. Proofreading-deficient CoVs with disrupted ExoN activity [ExoN(-)] are either non-viable or have significant defects in replication, RNA synthesis, fidelity, fitness, and virulence. In this study, we show that ExoN(-) murine hepatitis virus can adapt over long-term passage for increased replication and fitness without reverting the ExoN-inactivating mutations. Passage-adapted ExoN(-) mutants also demonstrate increasing resistance to nucleoside analogs that is only partially explained by secondary mutations in nsp12 and nsp14. These data suggest that enhanced resistance to nucleoside analogs is mediated by the interplay of multiple replicase proteins and support the proposed link between CoV fidelity and fitness.

INTRODUCTION

A paradigm of RNA virus biology is error-prone genomic replication due to the lack of proofreading or post-replicative RNA repair mechanisms (1-3). Decreased replication fidelity may constrain RNA genome size and complexity and risks the accumulation of deleterious mutations leading to population extinction, a process known as lethal mutagenesis (4-7). While genetic diversity allows viral populations to adapt rapidly under selective pressure, many mutations are neutral or detrimental to viral fitness (8-12). Research performed with many RNA viruses supports the hypothesis that the mutation rate of RNA virus replicases has evolved to balance multiple characteristics of the viral population such as genetic diversity, genomic integrity, and virulence. High- or low-fidelity variants are described for many RNA viruses infecting animals including the coronaviruses (CoVs): murine hepatitis virus (MHV-A59) and Severe Acute Respiratory Syndrome-associated coronavirus (SARS-CoV) (13-17), as well as foot-and-mouth disease virus {Arias:2008bp, Zeng:2013dg, Zeng:2014dj, Xie:2014cs, Sierra:2007dg}, poliovirus (23-29), chikungunya virus (30, 31), influenza virus (32), coxsackievirus B3 (33, 34), and human enterovirus 71 (35-37). Most altered-fidelity variants described to date harbor mutations within the viral RNA-dependent RNA polymerase (RdRp), are attenuated *in vivo*, and protect against reinfection, highlighting their potential utility as live-attenuated vaccines (24, 28, 29, 38, 39). These studies underscore the importance of understanding the molecular mechanisms by which RNA viruses regulate their replication fidelity.

Viruses in the family *Coronaviridae* have large single-stranded positive-sense RNA genomes [(+)ssRNA] (40), ranging between 25.4 and 33.5 kilobases in length (41, 42). CoVs encode a 3′→5′ exoribonuclease (ExoN) in the N-terminal half of nonstructural protein 14

78 (nsp14-ExoN) (43, 44). CoV ExoN activity requires the presence of conserved magnesium-
79 coordinating acidic amino acids in three motifs that together constitute the active site (DE-E-D)
80 (45). The CoV ExoN is grouped with the DE-D-Dh superfamily of exonucleases involved in
81 proofreading during prokaryotic and eukaryotic DNA replication (Fig. 1) (43-47). Alanine
82 substitution of CoV motif I DE residues (DE→AA) reduces biochemical ExoN activity in
83 SARS-CoV (45, 47) and human coronavirus 229E (43). MHV-A59 and SARS-CoV lacking
84 ExoN activity [ExoN(-)] have mutation frequencies 8-to-20-fold greater than WT viruses (13, 14,
85 38). Thus, all available data to date support the hypothesis that nsp14-ExoN is the first known
86 proofreading enzyme encoded by an RNA virus.
87 Despite the critical role of ExoN in virus replication, fidelity, fitness, and virulence,
88 ExoN(-) mutants have not reverted the inactivating substitutions (GAT→GCA – D89A;
89 GAA→GCT – E91A) (Fig. 1) (13, 14, 16, 17, 38). In fact, ExoN-inactivating mutations have
90 been retained during up to 20 passages in culture, eight acute passages of SARS-CoV-ExoN(-) in
91 aged BALB/c mice, and 60 days of persistent SARS-CoV-ExoN(-) infection in immunodeficient
92 Rag-/- mice. In this study, we sought to determine whether long-term passage of MHV-A59-
93 ExoN(-) (250 passages over one year; P250), hereafter MHV-ExoN(-), would result in virus
94 extinction, ExoN(-) reversion, or compensation for the loss of proofreading. We demonstrate that
95 MHV-ExoN(-) did not extinguish during the 250 passages and adapted in a gradual, continuous
96 process for increased replication. MHV-ExoN(-) concurrently evolved reduced susceptibility to
97 nucleoside and base analogs without reversion of the ExoN-inactivating mutations. The evolved
98 mutations in MHV-ExoN(-) nsp14 and nsp12, which encodes the RdRp, accounted for only part
99 of the increased replication and nucleoside analog resistance of MHV-ExoN(-) P250. This study
100 demonstrates a surprising stability of the ExoN-inactivating substitutions, suggests that CoVs can

evolve to compensate for the loss of ExoN functions, and indicates that proteins or other determinants outside of nsp12 and nsp14 likely contribute to CoV fidelity regulation.

RESULTS

Long-term passage of MHV-ExoN(-). We serially passaged WT-MHV and MHV-ExoN(-) in delayed brain tumor (DBT) cells 250 times (P250). Virus from each passage was harvested once 50-100% of the monolayer was involved in syncytia, which occurred between 8 and 24 hours post-infection. Passage conditions varied for WT-MHV and MHV-ExoN(-) due to differences in replication kinetics between the two viruses. We stopped passage at P250 after observing reduced syncytia formation in MHV-ExoN(-)-infected flasks, likely resulting from a mutation in the MHV-ExoN(-) P250 spike protein cleavage site (discussed below).

MHV-ExoN(-) and WT-MHV replicate with identical kinetics following 250 passages. MHV-ExoN(-) has a significant replication defect relative to WT-MHV (14). We first tested whether replication of MHV-ExoN(-) P250 was affected by long-term passage. MHV-ExoN(-) P3 replication was delayed by ~2 hours and peak titer reduced by ~1 $\log_{10}$ relative to WT-MHV P3 during high MOI infection (1 PFU/cell) (Fig. 2A, solid lines), consistent with our previous studies (14). By P250, both viruses replicated with identical kinetics (Fig. 2A, dotted lines). This represented a ~1 $\log_{10}$ increase in peak replication for WT-MHV and a ~2 $\log_{10}$ increase for MHV-ExoN(-), compared with the respective parental virus. Further, MHV-ExoN(-) P250 titers were maintained throughout the experiment, while WT-MHV P250 titers gradually decreased after 12 hours. We next performed infection at low MOI (0.01 PFU/cell) to examine replication over multiple cycles. Much like at MOI=1, WT-MHV P250 and MHV-ExoN(-) P250 replicated identically during multi-cycle infection, reaching peak titer around 28 hours post-infection (Fig. 2B). We also tested replication of MHV-ExoN(-) at P10, P50, P100, and P160. Replication kinetics gradually increased over passage, reaching P250-like levels by P100 (Fig. 2B). To

127 determine whether the increased replication of MHV-ExoN(-) P250 was affected by the presence
128 of potential defective viral genomes or by some other population-based phenomenon, both WT-
129 MHV P250 and MHV-ExoN(-) P250 were plaque purified three times. The plaque-purified
130 viruses replicated indistinguishably from the parent populations (Fig. 2C). Together, these data
131 demonstrate that WT-MHV and MHV-ExoN(-) populations adapted for increased replication and
132 that either individual genomes or those derived from a single virus plaque encoded the adaptive
133 changes required by the total population.
134
135 **MHV-ExoN(-) accumulated 8-fold more mutations than WT-MHV but did not revert**
136 **ExoN-inactivating mutations.** To determine whether primary reversion of nsp14-ExoN(-)
137 resulted in enhanced replication of MHV-ExoN(-) P250, we sequenced nsp14 from infected-cell
138 total RNA. MHV-ExoN(-) P250 retained the motif I DE→AA substitutions, and we did not
139 detect any variation in motif I at the level of di-deoxy sequencing at any passage, demonstrating
140 that phenotypic changes were not the result of primary reversion of ExoN(-) motif I. To identify
141 potentially adaptive consensus mutations, we performed full-genome di-deoxy sequencing of
142 MHV-ExoN(-) P250 and WT-MHV P250. Within WT-MHV P250, we identified 23 mutations,
143 of which 17 were nonsynonymous (NS) (Fig. 3A). In contrast, MHV-ExoN(-) P250 had 171 total
144 mutations (74 NS) (Fig. 3B). The full-genome sequences have been deposited in GenBank, and
145 the mutations for both viruses are listed in Supplemental Tables 1 and 2. We identified only one
146 mutation shared by both viruses (nsp1 A146T), though it was present in approximately 50% of
147 the WT-MHV P250 population by di-deoxy sequencing. Both viruses deleted most of the
148 hemagglutinin esterase (HE). In MHV-A59, HE mRNA is not transcribed *in vitro* (48-50), and
149 HE protein expression is detrimental to MHV-A59 fitness in cell culture (51). WT-MHV P250

also deleted ORF 4a, which is dispensable for MHV replication in cell culture (52). The C-terminal region of ns2 within MHV-ExoN(-) P250 was truncated and fused to HE with a -1 frameshift. Ns2 is a phosphodiesterase (PDE) that protects viral RNA by degrading 2′→5′ oligoadenylate, the activating factor for cellular RNase L (53-55). The portion of ns2 deleted in MHV-ExoN(-) P250 lies outside the PDE catalytic domain, in a region of unknown function. C-terminally truncated ns2 retains enzymatic activity (56), but whether this specific deletion and fusion disrupts PDE activity remains to be tested. Nevertheless, ns2 is dispensable for MHV replication in immortalized cells (57, 58). Details about the deletion sites are provided in Supplemental Figure 1. Within proteins predicted to be part of the replicase-transcriptase complex (nsp7-16 and nucleocapsid) (39), WT-MHV P250 had only one NS change, located in the nsp13-helicase (Fig. 3A). In contrast, MHV-ExoN(-) P250 had 17 NS changes within this region (Fig. 3B and Supplemental Tables 1, 2).

MHV-ExoN(-) P250 displays increased genomic RNA accumulation and increased resistance to 5-fluorouracil. Coronaviruses lacking ExoN consistently display defects in RNA synthesis relative to WT (14, 16, 43). To determine whether the increased replication of MHV-ExoN(-) P250 was associated with restored genomic RNA (gRNA) production, we measured gRNA accumulation over time using two-step real-time quantitative PCR (15, 16). MHV-ExoN(-) P250 accumulated similar levels of gRNA to WT-MHV P3 and WT-MHV P250 at early time points, while gRNA levels for MHV-ExoN(-) P3 were ~1 $\log_{10}$ lower (Fig. 4A). MHV-ExoN(-) P250 gRNA levels fell below those of WT-MHV and WT-MHV P250 after 8 hours and were similar to those of MHV-ExoN(-) P3 at 10 hours post-infection. Normalizing to the gRNA abundance at four hours for each virus demonstrated that the rates of gRNA accumulation were

similar for all four viruses (Fig. 4B). These data suggest that the increased replication of P250 viruses relative to WT-MHV is not fully accounted for by increased RNA synthesis. In addition to RNA synthesis defects, ExoN(-) CoVs have up-to 20-fold increased mutation frequencies and profoundly increased sensitivity to nucleoside and base analogs relative to WT CoVs (13, 14, 16, 17, 38). To determine whether nucleoside analog sensitivity of MHV-ExoN(-) was altered by long-term passage, we treated cells infected with parental and passaged viruses with the base analog, 5-fluorouracil (5-FU). 5-FU is converted intracellularly into a nucleoside analog that incorporates into growing RNA strands and causes A:G and U:C mutations. For simplicity, we hereafter refer to 5-FU as a nucleoside analog. Incorporation of 5-FU is increased in the absence of ExoN activity (16). All viruses displayed a concentration-dependent decrease in viral titer but differed greatly in their susceptibility to 5-FU (Fig. 4C). At 120μM, WT-MHV P3 titers were reduced by ~1 $\log_{10}$, while MHV-ExoN(-) P3 titers were undetectable (> 5 $\log_{10}$-fold reduction). WT-MHV 5-FU sensitivity was not altered by passage. MHV-ExoN(-) P250 was less susceptible than MHV-ExoN(-) P3 to 5-FU treatment, with only a ~1.5 $\log_{10}$ decrease in titer at 120 μM. MHV-ExoN(-) P250 remained more sensitive to 5-FU than WT-MHV, suggesting that WT-like resistance requires an intact ExoN. These data demonstrate that MHV-ExoN(-) P3 evolved resistance to 5-FU through mutations outside of ExoN(-) motif I.

Spike mutations in MHV-ExoN(-) P250 do not increase resistance to 5-FU. Bacteriophage ϕX174 acquired resistance to 5-FU by delaying cell lysis, thereby reducing the number of replication cycles in which 5-FU can be incorporated (59). MHV-ExoN(-) P250 had multiple mutations in the spike glycoprotein, including one in the spike furin cleavage site that reduced syncytia formation. To test whether the spike mutations manifested in resistance to 5-FU, we

196 cloned the spike gene from MHV-ExoN(-) P250 into the isogenic MHV-ExoN(-) background.
197 The recombinant virus demonstrated intermediate replication kinetics between MHV-ExoN(-) P3
198 and MHV-ExoN(-) P250 (Fig. 5A) and did not form syncytia. Spike-P250 also increased the
199 specific infectivity of viral particles (Fig. 5B). However, the MHV-ExoN(-) P250 spike did not
200 affect sensitivity of the recombinant virus to 5-FU (Fig. 5C). Thus, any adaptive increase in 5-FU
201 resistance must be located elsewhere in the genome.
202
203 **MHV-ExoN(-) passage resulted in unique mutations in nsp12 and nsp14.** To date, three
204 proteins have been shown to alter CoV sensitivity to 5-FU: the nsp12-RdRp, nsp14-ExoN, and
205 nsp10, which stimulates ExoN activity (15, 17, 39). Neither WT-MHV nor MHV-ExoN(-) P250
206 contained a NS mutation in nsp10, and WT-MHV P250 had no mutations within either nsp12 or
207 nsp14. In contrast, MHV-ExoN(-) P250 had 7 NS mutations in nsp12 and 6 NS mutations in
208 nsp14 (Figs. 3, 6), none of which have been described previously *in vitro* or in viable viruses.
209 Within nsp12, six mutations were in the predicted RdRp fingers, palm, and thumb domains (Fig.
210 6A) (60). Four residues (H709, F766, S776, and M814) can be visualized on a Phyre^2-modeled
211 structure of the MHV-nsp12 RdRp, while the remainder lie outside the modeled core RdRp (Fig.
212 6A) (17). One mutation, M288T, lies in the CoV-specific domain, which is conserved among
213 nidoviruses. This domain has been implicated in membrane targeting in MHV-A59 (61) and
214 performs an essential nucleotidylation activity in the arterivirus, equine arteritis virus (62).
215 However, M288T is not predicted to catalyze nucleotidylation. Within nsp14, 4 NS mutations
216 were identified in the ExoN domain, and 2 NS mutations were in the C-terminal N7-
217 methyltransferase domain (Fig. 6B). We next modeled the structure of MHV nsp14 using Phyre^2
218 software (63), resulting in highest-probability similarity to the SARS-CoV nsp14-nsp10 complex

(PDB: 5C8S) (45) with high-confidence (i.e. the calculated probability of true homology between the structures) of 100% for residues 3-519 of MHV-nsp14. The model predicts that five mutations are located close to surface of the protein (Fig. 6B). All three modeled zinc finger domains contain one NS mutation (F216Y, Y248H, L473I). Two mutations, D128E and F216Y, are located near the interface between nsp10 and nsp14, though neither site has previously been implicated in nsp10-nsp14 interaction (15, 64, 65). One NS mutation resulted in a D272E substitution in ExoN motif III, a metal-coordinating active site residue. We previously reported that alanine substitution of D272 results in an ExoN(-) phenotype (14), but the viability or phenotype of a D272E substitution was not tested in that study. These data suggest that a network of residues evolved to regulate nsp12 and nsp14 activity or stability in the ExoN(-) background.

Fixed mutations in nsp12 and nsp14 in MHV-ExoN(-) P250 directly correlate with increased resistance to multiple nucleoside analogs. To determine approximately when the mutations in nsp12 and nsp14 arose, we performed di-deoxy sequencing across these protein-coding regions roughly every 20 passages (P10, 31, 50, 72, 90, 100, 120, 140, 160, 180, 200, 220, 240). By this method, we detected consensus NS mutations at P10, P50, and P160 for nsp12, and at P50 and P160 for nsp14 (Fig. 6). Both nsp12 and nsp14 carried their full complement of P250 consensus mutations by P160, except for a minority variant (D913E) in nsp12 maintained at <50% of the population between P200 and P250. These passage levels correlated with increased replication of MHV-ExoN(-) (Fig. 2B) and with decreasing sensitivity to 5-FU (Fig. 7A). Neither replication nor 5-FU sensitivity of MHV-ExoN(-) changed substantially between P160 and P250. To determine whether MHV-ExoN(-) evolved increased resistance to multiple nucleoside

242 analogs, we treated virus-infected cells with three additional analogs that are substrates for viral
243 RdRps: ribavirin (RBV), a guanine analog that inhibits viral replication through multiple
244 mechanisms, including mutagenesis and inhibition of purine biosynthesis (66); 5-azacytidine
245 (AZC), an RNA mutagen (67); and 2'-C-methyladenosine (CMeA), which is proposed to
246 incorporate in viral RNA and terminate nascent transcripts (68). As with 5-FU, we observed
247 dose-dependent sensitivity to RBV, AZC, and CMeA in all MHV-ExoN(-) viruses that decreased
248 with increasing passage number (Fig. 7B-D). Except against AZC, MHV-ExoN(-) sensitivity did
249 not change between P160 and P250. Together, these data demonstrate that MHV-ExoN(-)
250 evolved increased resistance to multiple nucleoside analogs that correlated with the length of
251 passage and the acquisition of mutations in nsp12 and nsp14. Importantly, this occurred in the
252 absence of specific mutagenic selection and without reversion of ExoN motif I. This increased
253 general selectivity towards all four classes of nucleotide strongly advocates for an overall
254 increase in fidelity in MHV-ExoN(-) P250.
255
256 **Mutations in nsp12 partially account for increased resistance of MHV-ExoN(-) P250 to**
257 **multiple nucleoside analogs.** We hypothesized that mutations in MHV-ExoN(-) P250 nsp12 and
258 nsp14 were most likely to impact replication and nucleoside analog sensitivity based on their
259 enzymatic activities and temporal association with phenotypic changes. To test this hypothesis,
260 we engineered recombinant MHV-ExoN(-) to encode the P250 nsp12 and nsp14, alone and
261 together. Expression of nsp12-P250 and nsp14-P250, alone or in combination, altered replication
262 kinetics of MHV-ExoN(-) without affecting peak titers (Fig. 8A) and increased gRNA levels
263 above those of MHV-ExoN(-) P3 (Fig. 8B). Nsp12-P250 had a greater effect than nsp14-P250 on
264 the sensitivity of MHV-ExoN(-) to all analogs tested, and the combination of nsp12- and nsp14-

P250 did not increase resistance above nsp12-P250 alone (Fig. 8C-E). None of the recombinant viruses recapitulated the resistance phenotypes of the MHV-ExoN(-) P250 population. Together, these data demonstrate that nsp12-P250 mutations only partially account for the nucleoside analog resistance of MHV-ExoN(-) P250, and that adaptations in nsp12-P250 mask those in nsp14-P250. We also can conclude that the nsp14-P250 D272E active site mutation does not correct the defect caused by the motif I DE→AA substitutions. Together, the results suggest possible limitations for fidelity adaptation in nsp12 and nsp14, and also the exciting prospect that other CoV proteins participate in fidelity regulation within MHV-ExoN(-) P250.

Resistance to nucleoside analogs correlates with MHV-ExoN(-) fitness. We hypothesized that mutations in nsp12 and nsp14 provided a fitness advantage to MHV-ExoN(-) P250. We competed the recombinant viruses with a reference MHV-ExoN(-) virus (P1 stock) containing 10 silent mutations in the nsp2 coding region. Mutant and reference viruses were detected in the mixed infection by real-time quantitative PCR using dual-labeled probes specific for each virus. MHV-ExoN(-) P3 showed a modest fitness advantage over the reference P1 MHV-ExoN(-) silent (Fig. 8F, solid green). MHV-ExoN(-) P250 profoundly outcompeted MHV-ExoN(-) silent, with >1000-fold more MHV-ExoN(-) P250 genomes present at the end of passage 1 (Fig. 8F, dotted green). MHV-ExoN(-) nsp12-P250 had greater relative fitness than MHV-ExoN(-) nsp14-P250, and MHV-ExoN(-) nsp12/14-P250 was intermediate between the single recombinants, implicating a complex evolutionary interaction between these two proteins. The measured fitness correlated with the patterns of nucleoside analog resistance and RNA synthesis associated with mutations in nsp12 and nsp14, suggesting a link between the evolution of these virus phenotypes.

287 The result also confirms that nsp12 and nsp14 are important but not sufficient to account for the

288 significantly increased fitness of MHV-ExoN(-) P250 relative to MHV-ExoN(-) P3.

289

DISCUSSION

High-fidelity replication is proposed to be critical for maintaining the large (+)ssRNA genomes of CoVs (40, 69). Our previous studies demonstrate that ExoN-mediated proofreading is required for replicative fitness, nucleoside analog resistance, and virulence (16, 17, 38). Yet no direct test of the requirement for ExoN activity for long-term survival and stability of the CoV genome had been performed. In this study, we describe experimental adaptive evolution of WT-MHV and MHV-ExoN(-) during long-term passage in cell culture. WT-MHV evolved increased replication kinetics over 250 passages, with few consensus mutations arising in the WT-MHV P250 genome. In contrast, MHV-ExoN(-) accumulated 8-fold more mutations than WT-MHV, none of which occurred at the ExoN-inactivating mutations. Nevertheless, MHV-ExoN(-) P250 demonstrated increased replication kinetics and increased resistance to nucleoside analogs as compared to MHV-ExoN(-) P3. Mutations within nsp12-P250 conferred greater resistance to nucleoside analogs than nsp14-P250, suggesting that secondary mutations within nsp14 cannot restore ExoN activity without the full complement of catalytic DE-E-D residues. These results further support our studies and those from other exonucleases that the motif I DE residues are absolutely required for ExoN activity. However, mutations in nsp12-P250 also were not sufficient, alone or in combination with nsp14-P250, to account for the increased nucleoside analog resistance of the MHV-ExoN(-) P250 virus population, indicating that other proteins contribute to resistance or that the virus evolved increased mutational robustness over passage.

Why doesn't MHV-ExoN(-) revert over long-term passage? We detected no primary reversion at the DE→AA substitutions MHV-ExoN(-) at any passage tested. These data are consistent with and significantly extend previous studies reporting genotypic stability of ExoN(-)

313 motif I in MHV and SARS-CoV (13, 14, 16, 17, 38). Complete reversion within ExoN(-) motif I
314 to DE would require four nucleotide changes. This likely represents a high genetic barrier to
315 reversion, especially given that fitness can be increased by mutations outside of nsp14-ExoN.
316 Single and double nucleotide changes within motif I could restore acidic charge to individual
317 residues (e.g. motif I EA, AD, ED, etc). However, the active site compositions of DEDDh
318 exonucleases, such as the Klenow fragment, are so stringent that even conservative mutations
319 (D-to-E or E-to-D) reduce ExoN activity by >96% (70). Thus, intermediate amino acid changes
320 may not have a selective advantage compared to motif I AA, limiting the evolutionary pathways
321 to reversion. However, nsp14-P250 increased competitive fitness in the MHV-ExoN(-)
322 background (Fig. 8F), demonstrating a modest capacity for fitness adaptation in nsp14 outside of
323 the catalytic residues. Whether these mutations resulted from genetic drift or positive selection
324 remains unclear. Nevertheless, our data show that MHV-ExoN(-) can adapt for increased fitness
325 without fully restoring exoribonuclease activity. Understanding the mechanisms by which MHV-
326 ExoN(-) P250 compensated for ExoN activity could allow recovery of ExoN(-) variants of other
327 CoVs, such as transmissible gastroenteritis virus and human CoV 229E, which to date have been
328 unrecoverable as ExoN(-) recombinants (43, 71).
329
330 **CoV adaptation to loss of ExoN-mediated proofreading.** High-fidelity replication, made
331 possible in part by the proofreading activity of nsp14-ExoN, is thought to have been essential for
332 the expansion and maintenance of large CoV genomes (39, 40, 69). Compensation for the loss of
333 ExoN could have occurred through the evolution of increased fidelity via other replicase proteins.
334 Mutations conferring increased replication fidelity to RNA viruses have most frequently been
335 mapped to RdRps (24, 25, 30, 72). Three findings suggest that mutations within nsp12-P250

confer increased polymerase fidelity. First, nonsynonymous mutations to the RdRp arose in the low-fidelity MHV-ExoN(-) but not in the presence of proofreading (WT-MHV). Second, five of the mutations lie in or near structural motifs important for fidelity regulation in other RdRps. Amino acid substitutions in the fingers and palm domains have been repeatedly shown to affect viral RdRp fidelity (25, 34), and we have recently reported a fingers mutation (nsp12-V553I) that likely increases the fidelity of the MHV RdRp (17). Our modeled structure predicts that nsp12-P250 contains three mutations in the palm domain and one in the fingers domain, with the M814K thumb domain mutation lying near the palm (Fig. 6A). Third, exchange of nsp12-P250 alone into the background of MHV-ExoN(-) reduced the susceptibility of MHV-ExoN(-) to three different nucleoside analogs (Fig. 8). Although resistance to a single nucleoside analog can evolve without increasing overall fidelity, resistance to multiple nucleoside analogs suggests a broadly increased capacity to discriminate modified nucleotides {Arias:2008bp, Sierra:2007dg, Zeng:2013dg, Guo:2016fx}. Thus, nsp12-P250 is likely a high-fidelity polymerase. However, nsp12-P250 only partially accounts for the MHV-ExoN(-) P250 nucleoside analog resistance phenotype (Fig. 8), suggesting a possible limit to the compensation achievable by mutating the RdRp alone. Further, the effects of mutations in nsp12-P250 and nsp14-P250 are not additive and may be antagonistic when isolated from the whole passaged virus (Fig. 8), indicating that the relationships between nsp12- and nsp14-P250 mutations are likely evolutionarily linked with those in other MHV proteins. In fact, a substantial component of the evolved resistance to nucleoside analogs cannot be explained by nsp12-P250 and nsp14-P250, alone or together. In support of this hypothesis, we identified several nonsynonymous mutations in other replicase proteins, such as nsps 8, 9, 13, and 15. SARS-CoV nsp8 and nsp13 have functional interactions with nsp12, acting as a primase/processivity factor (74, 75) and a helicase/NTPase, respectively

359 (76). Processivity factors in herpes simplex virus and *Mycobacterium tuberculosis* regulate DNA
360 polymerase fidelity by balancing polymerase extension and exonuclease activity (77, 78), and
361 helicases in chikungunya virus and foot-and-mouth disease virus can evolve to increase fidelity
362 (79) and alter the frequency of ribavirin-induced mutations (80), respectively. SARS-CoV nsp9
363 has RNA-binding activities and is proposed to participate in the multi-protein replicase complex
364 (39, 81), and MHV nsp15 is a uridylate-specific endoribonuclease (82). Both could plausibly be
365 involved in modifying polymerase activity. Additionally, it remains possible that evolution for
366 increased fidelity could involve proteins outside the canonical replication complex (nsps7-16),
367 including those in the structural and accessory cassette. Thus, while immediate studies will focus
368 on testing whether replicase proteins nsp8, 9, 13, and 15 regulate fidelity, it is exciting to
369 consider the possibility that this virus-directed discovery approach will reveal novel interactions
370 between multiple MHV proteins.
371
372 **Has MHV-ExoN(-) P250 evolved robustness as a defense against ExoN(-) infidelity?** Three
373 of the nucleoside analogs used in this study (5-FU, ribavirin, and 5-azacytidine) reduce virus
374 titers at least in part through mutagenesis (16, 66, 67). Although the resistance of MHV-ExoN(-)
375 P250 to these RNA mutagens may be fully explained by the evolution of a high-fidelity
376 replication complex, an additional possibility is that MHV-ExoN(-) P3 evolved increased
377 mutational robustness. Mutational robustness is the capacity of a virus to buffer the fitness
378 effects of mutations, which are most frequently detrimental or lethal (8-12). Thus, in a low-
379 fidelity virus like MHV-ExoN(-) P3, genomic mutations which reduce the fitness cost of
380 subsequent mutations can provide a selective advantage (83-85). The relationship between
381 fidelity and robustness has been demonstrated for poliovirus and coxsackievirus B3: wild-type

poliovirus encodes a lower-fidelity polymerase than coxsackievirus and is more mutationally robust (86). Selection for increased robustness could explain the ~90 synonymous changes in MHV-ExoN(-) P250. Synonymous changes can alter codons to reduce the probability of non-conservative amino acid changes (87). Alternatively, the increased population size of MHV-ExoN(-) P250 could promote robustness by a "safety-in-numbers" effect, allowing efficient purging of low-fitness mutants while maintaining population fitness (88). Large populations also increase the likelihood of co-infection, allowing complementation between viral genomes. We did not observe an effect of increased replication in MHV-ExoN(-) P250 nucleoside analog resistance (Fig. 5), but a recent study with poliovirus suggests that mutagenized populations have elevated coinfection frequencies (89). Thus, complementation may contribute to MHV-ExoN(-) P250 nucleoside analog resistance. Conflicting evidence exists regarding whether mutational robustness itself affects the sensitivity to RNA mutagens (86, 87, 90); nevertheless, the robustness of MHV-ExoN(-) P250 merits further investigation.

Conclusions. One of the defining features of CoV replication is the proofreading activity of the nsp14 exoribonuclease that is a critical determinant of CoV replication, fidelity, and fitness. We here show that CoVs also have the capacity to compensate for loss of ExoN activity through a network of mutations in nsp12, nsp14, and elsewhere in the genome. Thus, while nsp14-ExoN appears to play a dominant role in CoV replication fidelity, its activity is likely closely tied to a highly evolved network of proteins. The demonstrated co-adaptation for replication, fidelity, and competitive fitness within MHV-ExoN(-) supports the hypothesis that these roles are linked functionally and evolutionarily. Genetic and biochemical testing of the rich mutational resource revealed in MHV-ExoN(-) P250 will likely inform the design of countermeasures for endemic

405 and emerging CoVs by defining novel common targets for stable virus attenuation or direct

406 inhibition.

407

MATERIALS AND METHODS

Cell culture. DBT-9 (delayed brain tumor, murine astrocytoma clone 9) cells were maintained as described previously (91). Baby hamster kidney (BHK) cells stably expressing the MHV-A59 receptor, CEACAM1, [BHK-R, (15)] were maintained under selection with 0.8 mg/ml of G418 (Mediatech) as described previously (91).

Long-term passage of virus and stock generation. The infectious cDNA clone for MHV-A59 and the recovery of MHV-ExoN(-) are described previously (14, 91). Long-term passage was initiated by infecting subconfluent monolayers of DBT-9 cells in 25 cm^2 flasks with either wild-type MHV-A59 or MHV-ExoN(-) at a multiplicity of infection (MOI) of approximately 0.1 particle forming unit per cell (PFU/cell). One lineage of each virus was passaged blindly for a total of 250 passages (P250). Supernatant was harvested at each passage and stored at -80°C. Total RNA was harvested for most passages using 1 ml of TRIzol Reagent (Ambion) per 25 cm^2 flask and stored at -80°C. Virus stocks of select intermediate passages were generated by infecting a subconfluent 150 cm^2 flask of DBT-9 cells at an MOI of 0.01 PFU/cell. Approximately 24 hours post-infection the flask was frozen at -80°C and the supernatant was clarified by centrifugation at 4,000 x g (Sorvall RC 3B Plus; HA-6000A rotor) for 10 min at 4°C. The virus titer of each stock was determined by plaque assay using DBT-9 cells as described previously (14, 91). For plaque assays of viruses containing the spike protein from MHV-ExoN(-) P250, which does not form syncytia, plaques were visualized with neutral red (Sigma #N6264, diluted 1:10 in PBS containing calcium and magnesium). Neutral red was added 24 hours after plating and incubated for an additional 3-8 hours before formaldehyde fixation. Plaque purification was performed by infecting DBT cells with serial dilutions of virus and overlaying

the cultures with agar. Single plaques were isolated, resuspended in PBS containing calcium and magnesium, and inoculated onto fresh DBTs. This process was completed 3 times before experimental stocks were generated, as above.

Sequencing of virus stocks. Following P250, RNA was purified from the harvested TRIzol samples according to the manufacturer's protocol and reverse transcribed (RT) using SuperScript III (Invitrogen) as described previously (14). Full-genome di-deoxy sequencing was performed for both WT-MHV P250 and MHV-ExoN(-) P250 using 12 overlapping amplicons approximately three kilobases in length. All coding regions were sequenced fully, and out of 31,409 nucleotides, > 99% were sequenced for each virus [WT-MHV P250: 21-31,279 and MHV-ExoN(-) P250: 21-31,275]. Two microliters of RT product were used for each PCR reaction (16). Di-deoxy sequencing was performed by Genhunter Corporation (Nashville, TN) or GENEWIZ (South Plainfield, NJ). Sequence analysis was performed using MacVector version 14 (MacVector, Inc.; Apex, North Carolina) using the MHV-A59 infectious clone reference genome (GenBank accession no. AY910861). The nucleotide sequences of the amplicon and sequencing primers are available upon request. Sequencing of nsp12 and nsp14 from intermediate passages was performed using TRIzol-purified RNA from infected monolayers and using the primers listed below. Primers 6M1F (5'-TTTTGGCGAGATGGTAGC-3') and 7M2R (5'-GGTAAGACAGTTTTAGGTGAG-3') were used to generate a 3,425 nucleotide amplicon containing all of nsp12. Primers 7M3F (5'-ATGCTTACCAACTATGAGC-3') and 8M3R (5'-CCGATTTGAATGGCGTAG-3') were used to generate a 2,713 nucleotide amplicon containing all of nsp14. The PCR conditions for these reactions are the same as those used to generate the amplicons used for full-genome sequencing (16).

454

455 **Replication and RNA synthesis kinetics**. Viral replication kinetics in DBT-9 cells were
456 determined at an MOI of 1 PFU/cell or MOI of 0.01 PFU/cell as described previously (15).
457 Supernatant (300 μL) was harvested at the indicated time points, and the virus titer was
458 determined by plaque assay. The accumulation of genomic RNA at an MOI of 1 PFU/cell was
459 measured by two-step real-time quantitative RT-PCR (RT-qPCR) using intracellular RNA that
460 was TRIzol-extracted at the time points indicated. RNA was reverse-transcribed using
461 SuperScript III (Invitrogen), and cDNA derived from intracellular positive-sense viral RNA was
462 measured using primers directed to nsp10. Values were normalized to levels of the endogenous
463 control glyceraldehyde-3-phosphate dehydrogenase (GAPDH). No mutations within the primer
464 binding sites emerged in either P250 population. The primers and amplification conditions are
465 the same as reported previously (15), except that the RT product was diluted 1:10 prior to use.
466 Samples were plated in technical duplicate to minimize well-to-well variation. Data are
467 presented as $2^{-\Delta CT}$, where ΔCT denotes CT (target, nsp10) minus CT (reference, GAPDH).

468

469 **Determination of specific infectivity.** Subconfluent monolayers of DBT-9 cells in 24-well
470 plates were infected with the indicated virus at an MOI of 1 PFU/cell, and supernatant was
471 harvested at 12 h.p.i. The levels of genomic RNA in supernatant were measured using one-step
472 real-time quantitative RT-PCR (RT-qPCR) on TRIzol-extracted RNA as described previously
473 (17). Briefly, genomic RNA was detected with a 5' 6-carboxyfluorescein (FAM) and 3' black
474 hole quencher 1 (BHQ-1) labeled probe targeting nsp2 (Biosearch Technologies, Petaluma, CA),
475 and RNA copy number was calculated by reference to an RNA standard derived from the MHV
476 A fragment. Samples were plated in technical duplicate to minimize well-to-well variation. Titers

were determined by plaque assay in DBT-9 cells, and specific infectivity was calculated as PFU per supernatant genomic RNA copy.

Nucleoside and base analog sensitivity assays. 5-azacytidine (AZC), 5-fluorouracil (5-FU), and ribavirin (RBV) were purchased from Sigma (product numbers A2385, F6627, and R9644, respectively). Stock solutions of 5-FU and RBV were prepared in dimethyl sulfoxide (DMSO). 2'-C-methyladenosine (CMeA) was received from Gilead Sciences, Inc (Foster City, CA). Sensitivity assays were performed as described previously (16), except in 24-well plates at an MOI of 0.01 PFU/cell. Supernatants were harvested at 24 hours post-infection, and titers were determined by plaque assay.

Phyre^2-modeling of MHV-nsp14. The MHV nsp14 structure was modeled with the Phyre^2 online program (63) using nsp14 residues 3-519, corresponding to residues 6056-6573 of the ORF1ab polyprotein. The model was analyzed using the Pymol Molecular Graphics System, Version (Schrödinger, LLC).

Generation of nsp12 and nsp14 swaps. Viruses containing nsp12, nsp14, or nsp12 and nsp14 from MHV-ExoN(-) P250 were generated using the MHV-A59 reverse genetics system (91). RNA from the MHV-ExoN(-) P250 virus was reversed transcribed with SuperScript III (Invitrogen) and used to generate amplicons containing either nsp12 or nsp14. Each amplicon was flanked by 15 bp that overlapped with an amplicon generated from the backbone plasmid. Amplicons were inserted into MHV-A59 fragments using the InFusion HD Cloning kit (Takara Bio USA, Inc, Mountain View, CA). Nsp12 is split across MHV E and F, while nsp14 is

contained within MHV F. Reaction mixtures contained 50ng of vector, 200ng of insert, and 2μL of enzyme and were incubated for 15 minutes at 50°C. Errors were corrected by site-directed mutagenesis using Pfu Turbo polymerase (Agilent, Santa Clara, CA). The nsp12/14-P250 swap was generated through restriction digestion of the individual swaps using BsmBI and StuI followed by gel purification and assembly using T4 DNA ligase (NEB, Ipswich, MA). Viable viruses were constructed and rescued as described previously (91).

Competitive fitness assays. Competitor viruses were competed with an MHV-ExoN(-) virus harboring 10 silent mutations in the probe-binding region within nsp2. Subconfluent DBT-9 monolayers in 24-well plates were coinfected at a total MOI of 0.01 PFU/cell with competitor and reference viruses at a 1:1 ratio and passaged 4 times. For each passage, supernatants were harvested at 24 hours. RNA was extracted from 100μL of supernatant using 900μL of TRIzol reagent and PureLink RNA Mini Kit columns (Thermo Scientific, Waltham, MA), and 150μL was used to infect fresh cells in a 24-well plate (total MOI estimated at 1 PFU/cell). The proportion of each virus was determined by real-time RT-qPCR from the infection supernatant using two Taqman probes with different fluorescent dyes in separate reactions. Competitor viruses were detected with the same probe used in specific infectivity analyses (14). Reference viruses were detected by a probe targeting the same region but with 10 silent mutations (5'-TCCGAACTACTGCAACCCCAAGTG-3') and labeled with 5' Quasar 670 and 3' black hole quencher 2 (BHQ-2) (Biosearch Technologies, Petaluma, CA). RNA copy number was calculated by reference to an RNA standard generated by *in vitro* transcription of the corresponding MHV A fragment, and relative RNA abundance was calculated as the ratio of competitor genomes to reference genomes.

Statistical analysis. GraphPad Prism 6 (La Jolla, CA) was used to perform statistical tests. Only the comparisons shown [e.g. ns or asterisk(s)] within the figure or legend were performed. In many cases the data were normalized to untreated controls. This was performed using GraphPad Prism 6. The number of replicate samples is denoted within each figure legend.

Accession numbers. Full-length genome sequences for WT-MHV P250 and MHV-ExoN(-) P250 have been deposited in GenBank (accession numbers MF618252 and MF618253, respectively).

ACKNOWLEDGEMENTS

We thank members of the Denison laboratory for valuable discussions. This work was supported by United States Public Health Service awards R01-AI108197 (M.R.D), T32-GM007347 (K.W.G), F30-AI129229 (K.W.G), T32-HL07751 (J.B.C), T32-AI089554 (N.R.S.), T32-AI095202 (E.C.S.), and F32-AI108102 (E.C.S.), all from the National Institutes of Health. The content is solely the responsibility of the authors and does not necessarily represent the official views of the National Institutes of Health. The authors declare no conflicts of interest.

FIGURE LEGENDS

Figure 1. MHV genome organization and nsp14 exoribonuclease motifs. (*Top*) The MHV genome is a 31.4kb, capped (dark circle), and polyadenylated positive sense RNA molecule. The first two thirds of the genome encode 16 nonstructural proteins translated as a single polyprotein with a ribosomal frameshift. The final one third encodes the structural proteins. (*Inset*) Nsp14 encodes an exoribonuclease (solid blue) and N7-methyltransferase (hatched blue) and has 3 zinc fingers (gray boxes) predicted from the solved SARS nsp10/14 crystal structure (PDB 5C8U) (45). Catalytic residues for ExoN are marked with white boxes, and the engineered mutations for MHV-ExoN(-) are shown below the genome. The nsp12 RNA-dependent RNA polymerase is highlighted in red.

Figure 2. MHV-ExoN(-) evolved increased replicative capacity over long-term passage. Replication curves were performed for the indicated viruses during high MOI (1 PFU/cell) (*A*) and low MOI (0.01 PFU/cell) (*B*) infections. (*C*) WT-MHV P250 and MHV-ExoN(-) P250 were plaque purified three times, and replication curves were performed in parallel with the full population (MOI = 0.01 PFU/cell. Supernatants were collected at the indicated times post infection, and titers were determined by plaque assay. Data for *A*-*C* represent mean and standard deviation of n = 3.

Figure 3. Mutation locations within passaged viruses. Mutations present at >50% by di-deoxy sequencing at passage 250 in WT-MHV (*A*) and MHV-ExoN(-) (*B*). Nonsynonymous mutations (red), noncoding mutations (cyan), and deletions (green boxes) are plotted above the schematic,

564 and synonymous mutations (purple) are below.

565

566 **Figure 4. MHV-ExoN(-) P250 has increased genomic RNA accumulation and increased**
567 **resistance to 5-fluorouracil.** (*A*) Cells were infected with the indicated viruses at MOI = 1
568 PFU/cell, and intracellular RNA was harvested using TRIzol at the indicated times post infection.
569 MHV genomic RNA was detected using SYBR green and primers directed to nsp10, and values
570 were normalized to intracellular GAPDH. (*B*) Same data as in panel (*A*) normalized to RNA
571 level for each virus at 4 hours post infection. Data represent mean and standard error for n = 9 (3
572 triplicate experiments). (*C*) Sensitivity of passaged viruses to 5-FU during low MOI infection
573 (0.01 PFU/cell). Cells were treated with the indicated concentrations of 5-FU for 30 minutes
574 prior to infection, and supernatants were harvested at 24 hours post-infection and titered by
575 plaque assay. Data represent change in titer relative to untreated control and plotted as mean and
576 standard error of n = 6 (two triplicate experiments). For panel C, statistical significance for
577 change in titer of MHV-ExoN(-) P250 relative to MHV-ExoN(-) P3 was determined Mann-
578 Whitney test (*P<0.05, **<0.01, ***P<0.001).

579

580 **Figure 5. Mutations in the spike envelope protein from MHV-ExoN(-) P250 increase**
581 **replicative capacity but do not affect sensitivity to 5-fluorouracil.** (*A*) Replication kinetics of
582 indicated viruses (MOI = 0.01 PFU/cell) plotted as mean and standard deviation with n = 3. (*B*)
583 Specific infectivity of indicated viruses 12 hours post-infection (MOI = 1 PFU/cell). Data
584 represent mean and standard error of n = 6 (two triplicate experiments). (*C*) Sensitivity of
585 indicated viruses to 5-fluorouracil during low MOI infection (0.01 PFU/cell), as described in Fig.
586 4. Data represent mean and standard error of n = 6 (two triplicate experiments). For panel B,

statistical significance was determined using one-way ANOVA. For Panel C, statistical significance for change in titer of MHV-ExoN(-) spike-P250 relative to MHV-ExoN(-) P3 was determined using Mann-Whitney test (*P<0.05, **<0.01, ***P<0.001, ns = not significant).

Figure 6. The timing of fixation of mutations in nsp12-RdRp and nsp14-ExoN within MHV-ExoN(-) correlates with increased resistance to nucleoside analogs. (*A*) A schematic of nsp12-RdRp with the CoV-specific region and the canonical fingers, palm, and thumb domains of RdRps is shown. The nsp12-RdRp coding region was sequenced at the indicated passage, and the nonsynonymous changes are plotted; gray boxes indicate consensus changes, and hatched boxes indicate variants present at <50% of the population by di-deoxy sequencing. At right, mutations are marked in orange on a Phyre^2-modeled structure of MHV-nsp12, with the active site residues marked in yellow (17). RdRp domains are colored according to the linear schematic. *NB*: M288T, L376P, and D913E lie outside the modeled region and thus are not marked. (*B*) A schematic of nsp14 with the ExoN and N7-methyltransferase domains is shown, with mutation plotting as in panel A. The black box denotes a mutation to ExoN motif III. At right, mutations are marked in orange on a Phyre^2-modeled structure of the MHV-nsp14/nsp10 complex. Domains are colored according to the linear schematic.

Figure 7. MHV-ExoN(-) evolved increased resistance to nucleoside and base analogs over passage. Sensitivity of isogenic and passaged viruses to the nucleoside analogs, 5-FU (*A*), ribavirin (*B*), 5-azacytidine (*C*), and 2'-C-methyladenosine (*D*) during low MOI infection (0.01 PFU/cell) as described in Fig. 4. Data represent mean and standard error for n = 6 (2 triplicate experiments). *NB*: Data for WT-MHV, WT-MHV P250, MHV-ExoN(-) P3, MHV-ExoN(-) P250

610 in panel (*A*) are the same as shown in Fig. 4C. Statistical significance for change in titer of
611 MHV-ExoN(-) P3 relative to MHV-ExoN(-) P250 was determined using Mann-Whitney test
612 (*P<0.05, **<0.01, ***P<0.001).
613
614 **Figure 8. Mutations in nsp12-RdRp and nsp14-ExoN from MHV-ExoN(-) P250**
615 **incompletely increase resistance to RNA mutagens and increase fitness of MHV-ExoN(-).**
616 (*A*) Replication kinetics of recombinant P250 viruses (MOI = 0.01 PFU/cell) plotted as mean and
617 standard deviation with n = 3. (*B*) Genomic RNA accumulation relative to intracellular GAPDH,
618 as described in Fig. 4. Data represent mean and standard error for n = 6-9 (2-3 triplicate
619 experiments). (*C-E*) Sensitivity of recombinant MHV-ExoN(-) viruses to 5-FU (*C*), ribavirin (*D*),
620 and 5-azacytidine (*E*) during low MOI infection (0.01 PFU/cell) as described in Fig. 4. Data
621 represent mean and standard error of n = 6. (*F*) Recombinant viruses were competed against a
622 reference MHV-ExoN(-) containing 10 silent mutations within nsp2. The ratio of viral genome
623 copies relative to the MHV-ExoN(-) reference is plotted. Data represent mean and standard error
624 of n = 6. *NB*: MHV-ExoN(-) P250 data set contains 4 replicates at passage 3 and a single
625 replicate at passage 4 due to undetectable levels of MHV-ExoN(-) silent. For panels C-E,
626 statistical significance for change in titer of swapped viruses relative to MHV-ExoN(-) P3 at
627 highest drug concentration tolerated was determined using Mann-Whitney test (*P<0.05,
628 **<0.01, ***P<0.001, ns = not significant). For panel F, statistical significance for the indicated
629 comparisons was determined using Mann-Whitney test. Boxed points have the same P value.
630
631 **Supplemental Figure 1. Deleted regions within WT-MHV P250 and MHV-ExoN(-) P250.**
632

REFERENCES

1. **Steinhauer DA**, **Domingo E**, **Holland JJ**. 1992. Lack of evidence for proofreading mechanisms associated with an RNA virus polymerase. Gene **122**:281–288.

2. **Sanjuán R**, **Nebot MR**, **Chirico N**, **Mansky LM**, **Belshaw R**. 2010. Viral mutation rates. J Virol **84**:9733–9748.

3. **Drake JW**, **Holland JJ**. 1999. Mutation rates among RNA viruses. Proc Natl Acad Sci USA **96**:13910–13913.

4. **Bull JJ**, **Sanjuán R**, **Wilke CO**. 2007. Theory of lethal mutagenesis for viruses. J Virol **81**:2930–2939.

5. **Domingo E**, **Sheldon J**, **Perales C**. 2012. Viral quasispecies evolution. Microbiol Mol Biol Rev **76**:159–216.

6. **Bradwell K**, **Combe M**, **Domingo-Calap P**, **Sanjuán R**. 2013. Correlation between mutation rate and genome size in riboviruses: mutation rate of bacteriophage Qβ. Genetics **195**:243–251.

7. **Gago S**, **Elena SF**, **Flores R**, **Sanjuán R**. 2009. Extremely high mutation rate of a hammerhead viroid. Science **323**:1308–1308.

8. **Peris JB**, **Davis P**, **Cuevas JM**, **Nebot MR**, **Sanjuán R**. 2010. Distribution of Fitness Effects Caused by Single-Nucleotide Substitutions in Bacteriophage f1. Genetics **185**:603–609.

9. **Malpica JM**, **Fraile A**, **Moreno I**, **Obies CI**, **Drake JW**, **García-Arenal F**. 2002. The

653 rate and character of spontaneous mutation in an RNA virus. Genetics **162**:1505–1511.

654 10. **Elena SF**, **Moya A**. 1999. Rate of deleterious mutation and the distribution of its effects
655 on fitness in vesicular stomatitis virus. Journal of Evolutionary Biology **12**:1078–1088.

656 11. **Visher E**, **Whitefield SE**, **McCrone JT**, **Fitzsimmons W**, **Lauring AS**. 2016. The
657 Mutational Robustness of Influenza A Virus. PLoS Pathog **12**:e1005856–25.

658 12. **Sanjuán R**, **Moya A**, **Elena SF**. 2004. The distribution of fitness effects caused by single-
659 nucleotide substitutions in an RNA virus. Proc Natl Acad Sci USA **101**:8396–8401.

660 13. **Eckerle LD**, **Becker MM**, **Halpin RA**, **Li K**, **Venter E**, **Lu X**, **Scherbakova S**, **Graham**
661 **RL**, **Baric RS**, **Stockwell TB**, **Spiro DJ**, **Denison MR**. 2010. Infidelity of SARS-CoV
662 Nsp14-exonuclease mutant virus replication is revealed by complete genome sequencing.
663 PLoS Pathog **6**:e1000896.

664 14. **Eckerle LD**, **Lu X**, **Sperry SM**, **Choi L**, **Denison MR**. 2007. High fidelity of murine
665 hepatitis virus replication is decreased in nsp14 exoribonuclease mutants. J Virol
666 **81**:12135–12144.

667 15. **Smith EC**, **Case JB**, **Blanc H**, **Isakov O**, **Shomron N**, **Vignuzzi M**, **Denison MR**. 2015.
668 Mutations in coronavirus nonstructural protein 10 decrease virus replication fidelity. J
669 Virol **89**:6418–6426.

670 16. **Smith EC**, **Blanc H**, **Surdel MC**, **Vignuzzi M**, **Denison MR**. 2013. Coronaviruses
671 lacking exoribonuclease activity are susceptible to lethal mutagenesis: evidence for
672 proofreading and potential therapeutics. PLoS Pathog **9**:e1003565.

673 17. **Sexton NR**, **Smith EC**, **Blanc H**, **Vignuzzi M**, **Peersen OB**, **Denison MR**. 2016.
674 Homology-Based Identification of a Mutation in the Coronavirus RNA-Dependent RNA
675 Polymerase That Confers Resistance to Multiple Mutagens. J Virol **90**:7415–7428.

676 18. **Arias A**, **Arnold JJ**, **Sierra M**, **Smidansky ED**, **Domingo E**, **Cameron CE**. 2008.
677 Determinants of RNA-dependent RNA polymerase (in)fidelity revealed by kinetic
678 analysis of the polymerase encoded by a foot-and-mouth disease virus mutant with
679 reduced sensitivity to ribavirin. J Virol **82**:12346–12355.

680 19. **Zeng J**, **Wang H**, **Xie X**, **Yang D**, **Zhou G**, **Yu L**. 2013. An increased replication fidelity
681 mutant of foot-and-mouth disease virus retains fitness in vitro and virulence in vivo.
682 Antiviral Res **100**:1–7.

683 20. **Zeng J**, **Wang H**, **Xie X**, **Li C**, **Zhou G**, **Yang D**, **Yu L**. 2014. Ribavirin-resistant
684 variants of foot-and-mouth disease virus: the effect of restricted quasispecies diversity on
685 viral virulence. J Virol **88**:4008–4020.

686 21. **Xie X**, **Wang H**, **Zeng J**, **Li C**, **Zhou G**, **Yang D**, **Yu L**. 2014. Foot-and-mouth disease
687 virus low-fidelity polymerase mutants are attenuated. Arch Virol **159**:2641–2650.

688 22. **Sierra M**, **Airaksinen A**, **González-López C**, **Agudo R**, **Arias A**, **Domingo E**. 2007.
689 Foot-and-mouth disease virus mutant with decreased sensitivity to ribavirin: implications
690 for error catastrophe. J Virol **81**:2012–2024.

691 23. **Vignuzzi M**, **Stone JK**, **Arnold JJ**, **Cameron CE**, **Andino R**. 2006. Quasispecies
692 diversity determines pathogenesis through cooperative interactions in a viral population.
693 Nature **439**:344–348.

694 24. **Vignuzzi M**, **Wendt E**, **Andino R**. 2008. Engineering attenuated virus vaccines by
695 controlling replication fidelity. Nat Med **14**:154–161.

696 25. **Pfeiffer JK**, **Kirkegaard K**. 2003. A single mutation in poliovirus RNA-dependent RNA
697 polymerase confers resistance to mutagenic nucleotide analogs via increased fidelity. Proc
698 Natl Acad Sci USA **100**:7289–7294.

699 26. **Arnold JJ**, **Vignuzzi M**, **Stone JK**, **Andino R**, **Cameron CE**. 2005. Remote site control
700 of an active site fidelity checkpoint in a viral RNA-dependent RNA polymerase. J Biol
701 Chem **280**:25706–25716.

702 27. **Liu X**, **Yang X**, **Lee CA**, **Moustafa IM**, **Smidansky ED**, **Lum D**, **Arnold JJ**, **Cameron**
703 **CE**, **Boehr DD**. 2013. Vaccine-derived mutation in motif D of poliovirus RNA-dependent
704 RNA polymerase lowers nucleotide incorporation fidelity. J Biol Chem **288**:32753–32765.

705 28. **Weeks SA**, **Lee CA**, **Zhao Y**, **Smidansky ED**, **August A**, **Arnold JJ**, **Cameron CE**.
706 2012. A Polymerase mechanism-based strategy for viral attenuation and vaccine
707 development. J Biol Chem **287**:31618–31622.

708 29. **Korboukh VK**, **Lee CA**, **Acevedo A**, **Vignuzzi M**, **Xiao Y**, **Arnold JJ**, **Hemperly S**,
709 **Graci JD**, **August A**, **Andino R**, **Cameron CE**. 2014. RNA virus population diversity, an
710 optimum for maximal fitness and virulence. J Biol Chem **289**:29531–29544.

711 30. **Coffey LL**, **Beeharry Y**, **Bordería AV**, **Blanc H**, **Vignuzzi M**. 2011. Arbovirus high
712 fidelity variant loses fitness in mosquitoes and mice. Proc Natl Acad Sci USA **108**:16038–
713 16043.

714 31. **Rozen-Gagnon K**, **Stapleford KA**, **Mongelli V**, **Blanc H**, **Failloux A-B**, **Saleh M-C**,
715 **Vignuzzi M**. 2014. Alphavirus mutator variants present host-specific defects and
716 attenuation in mammalian and insect models. PLoS Pathog **10**:e1003877.

717 32. **Cheung PPH**, **Watson SJ**, **Choy K-T**, **Fun Sia S**, **Wong DDY**, **Poon LLM**, **Kellam P**,
718 **Guan Y**, **Malik Peiris JS**, **Yen H-L**. 2014. Generation and characterization of influenza
719 A viruses with altered polymerase fidelity. Nat Commun **5**:4794.

720 33. **Gnädig NF**, **Beaucourt S**, **Campagnola G**, **Bordería AV**, **Sanz-Ramos M**, **Gong P**,
721 **Blanc H**, **Peersen OB**, **Vignuzzi M**. 2012. Coxsackievirus B3 mutator strains are
722 attenuated in vivo. Proc Natl Acad Sci USA **109**:E2294–303.

723 34. **Campagnola G**, **McDonald S**, **Beaucourt S**, **Vignuzzi M**, **Peersen OB**. 2015. Structure-
724 Function Relationships Underlying the Replication Fidelity of Viral RNA-Dependent
725 RNA Polymerases. J Virol **89**:275–286.

726 35. **Sadeghipour S**, **McMinn PC**. 2013. A study of the virulence in mice of high copying
727 fidelity variants of human enterovirus 71. Virus Research **176**:265–272.

728 36. **Sadeghipour S**, **Bek EJ**, **McMinn PC**. 2013. Ribavirin-resistant mutants of human
729 enterovirus 71 express a high replication fidelity phenotype during growth in cell culture.
730 J Virol **87**:1759–1769.

731 37. **Meng T**, **Kwang J**. 2014. Attenuation of human enterovirus 71 high-replication-fidelity
732 variants in AG129 mice. J Virol **88**:5803–5815.

733 38. **Graham RL**, **Becker MM**, **Eckerle LD**, **Bolles M**, **Denison MR**, **Baric RS**. 2012. A live,

734 impaired-fidelity coronavirus vaccine protects in an aged, immunocompromised mouse
735 model of lethal disease. Nat Med **18**:1820–1826.

736 39. **Smith EC**, **Sexton NR**, **Denison MR**. 2014. Thinking Outside the Triangle: Replication
737 Fidelity of the Largest RNA Viruses. Annual Review of Virology **1**:111–132.

738 40. **Gorbalenya AE**, **Enjuanes L**, **Ziebuhr J**, **Snijder EJ**. 2006. Nidovirales: evolving the
739 largest RNA virus genome. Virus Research **117**:17–37.

740 41. **Brister JR**, **Ako-Adjei D**, **Bao Y**, **Blinkova O**. 2014. NCBI Viral Genomes Resource.
741 Nucleic Acids Res **43**:gku1207–D577.

742 42. **Stenglein MD**, **Jacobson ER**, **Wozniak EJ**, **Wellehan JFX**, **Kincaid A**, **Gordon M**,
743 **Porter BF**, **Baumgartner W**, **Stahl S**, **Kelley K**, **Towner JS**, **DeRisi JL**. 2014. Ball
744 Python Nidovirus: a Candidate Etiologic Agent for Severe Respiratory Disease in Python
745 regius. MBio **5**:e01484–14–e01484–14.

746 43. **Minskaia E**, **Hertzig T**, **Gorbalenya AE**, **Campanacci V**, **Cambillau C**, **Canard B**,
747 **Ziebuhr J**. 2006. Discovery of an RNA virus 3"->5" exoribonuclease that is critically
748 involved in coronavirus RNA synthesis. Proc Natl Acad Sci USA **103**:5108–5113.

749 44. **Snijder EJ**, **Bredenbeek PJ**, **Dobbe JC**, **Thiel V**, **Ziebuhr J**, **Poon LLM**, **Guan Y**,
750 **Rozanov M**, **Spaan WJM**, **Gorbalenya AE**. 2003. Unique and conserved features of
751 genome and proteome of SARS-coronavirus, an early split-off from the coronavirus group
752 2 lineage. J Mol Biol **331**:991–1004.

753 45. **Ma Y**, **Wu L**, **Shaw N**, **Gao Y**, **Wang J**, **Sun Y**, **Lou Z**, **Yan L**, **Zhang R**, **Rao Z**. 2015.

754 Structural basis and functional analysis of the SARS coronavirus nsp14-nsp10 complex.
755 Proc Natl Acad Sci USA **112**:9436–9441.

756 46. **Zuo Y**, **Deutscher MP**. 2001. Exoribonuclease superfamilies: structural analysis and
757 phylogenetic distribution. Nucleic Acids Res **29**:1017–1026.

758 47. **Bouvet M**, **Imbert I**, **Subissi L**, **Gluais L**, **Canard B**, **Decroly E**. 2012. RNA 3'-end
759 mismatch excision by the severe acute respiratory syndrome coronavirus nonstructural
760 protein nsp10/nsp14 exoribonuclease complex. Proc Natl Acad Sci USA **109**:9372–9377.

761 48. **Yokomori K**, **Banner LR**, **Lai MMC**. 1991. Heterogeneity of gene expression of the
762 hemagglutinin-esterase (HE) protein of murine coronaviruses. Virology **183**:647–657.

763 49. **Luytjes W**, **Bredenbeek PJ**, **Noten AF**, **Horzinek MC**, **Spaan WJ**. 1988. Sequence of
764 mouse hepatitis virus A59 mRNA 2: indications for RNA recombination between
765 coronaviruses and influenza C virus. Virology **166**:415–422.

766 50. **Yokomori K**, **Lai MM**. 1991. Mouse hepatitis virus S RNA sequence reveals that
767 nonstructural proteins ns4 and ns5a are not essential for murine coronavirus replication. J
768 Virol **65**:5605–5608.

769 51. **Lissenberg A**, **Vrolijk MM**, **van Vliet ALW**, **Langereis MA**, **de Groot-Mijnes JDF**,
770 **Rottier PJM**, **de Groot RJ**. 2005. Luxury at a Cost? Recombinant Mouse Hepatitis
771 Viruses Expressing the Accessory Hemagglutinin Esterase Protein Display Reduced
772 Fitness In Vitro. J Virol **79**:15054–15063.

773 52. **Gadlage MJ**, **Graham RL**, **Denison MR**. 2008. Murine coronaviruses encoding nsp2 at

774 different genomic loci have altered replication, protein expression, and localization. J
775 Virol **82**:11964–11969.

776 53. **Zhao L**, **Jha BK**, **Wu A**, **Elliott R**, **Ziebuhr J**, **Gorbalenya AE**, **Silverman RH**, **Weiss**
777 **SR**. 2012. Antagonism of the Interferon-Induced OAS-RNase L Pathway by Murine
778 Coronavirus ns2 Protein Is Required for Virus Replication and Liver Pathology. Cell Host
779 and Microbe **11**:607–616.

780 54. **Li Y**, **Weiss SR**. 2016. Antagonism of RNase L is required for murine coronavirus
781 replication in Kupffer cells and liver sinusoidal endothelial cells but not in hepatocytes. J
782 Virol JVI.01423–16–24.

783 55. **Zhang R**, **Jha BK**, **Ogden KM**, **Dong B**, **Zhao L**, **Elliott R**, **Patton JT**, **Silverman RH**,
784 **Weiss SR**. 2013. Homologous 2“,5-”phosphodiesterases from disparate RNA viruses
785 antagonize antiviral innate immunity. Proc Natl Acad Sci USA **110**:13114–13119.

786 56. **Sui B**, **Huang J**, **Jha BK**, **Yin P**, **Zhou M**, **Fu ZF**, **Silverman RH**, **Weiss SR**, **Peng G**,
787 **Zhao L**. 2016. Crystal structure of the mouse hepatitis virus ns2 phosphodiesterase
788 domain that antagonizes RNase L activation. J Gen Virol **97**:880–886.

789 57. **Schwarz B**, **Routledge E**, **Siddell SG**. 1990. Murine coronavirus nonstructural protein
790 ns2 is not essential for virus replication in transformed cells. J Virol **64**:4784–4791.

791 58. **Zhao L**, **Rose KM**, **Elliott R**, **Van Rooijen N**, **Weiss SR**. 2011. Cell-type-specific type I
792 interferon antagonism influences organ tropism of murine coronavirus. J Virol **85**:10058–
793 10068.

794 59. **Pereira-Gómez M**, **Sanjuán R**. 2014. Delayed lysis confers resistance to the nucleoside
795 analogue 5-fluorouracil and alleviates mutation accumulation in the single-stranded DNA
796 bacteriophage ϕX174. J Virol **88**:5042–5049.

797 60. **Ng KKS**, **Arnold JJ**, **Cameron CE**. 2008. Structure-function relationships among RNA-
798 dependent RNA polymerases. Curr Top Microbiol Immunol **320**:137–156.

799 61. **Brockway SM**, **Clay CT**, **Lu XT**, **Denison MR**. 2003. Characterization of the expression,
800 intracellular localization, and replication complex association of the putative mouse
801 hepatitis virus RNA-dependent RNA polymerase. J Virol **77**:10515–10527.

802 62. **Lehmann KC**, **Gulyaeva A**, **Zevenhoven-Dobbe JC**, **Janssen GMC**, **Ruben M**,
803 **Overkleeft HS**, **van Veelen PA**, **Samborskiy DV**, **Kravchenko AA**, **Leontovich AM**,
804 **Sidorov IA**, **Snijder EJ**, **Posthuma CC**, **Gorbalenya AE**. 2015. Discovery of an
805 essential nucleotidylating activity associated with a newly delineated conserved domain in
806 the RNA polymerase-containing protein of all nidoviruses. Nucleic Acids Res **43**:8416–
807 8434.

808 63. **Kelley LA**, **Mezulis S**, **Yates CM**, **Wass MN**, **Sternberg MJE**. 2015. The Phyre2 web
809 portal for protein modeling, prediction and analysis. Nat Protoc **10**:845–858.

810 64. **Bouvet M**, **Lugari A**, **Posthuma CC**, **Zevenhoven JC**, **Bernard S**, **Betzi S**, **Imbert I**,
811 **Canard B**, **Guillemot J-C**, **Lécine P**, **Pfefferle S**, **Drosten C**, **Snijder EJ**, **Decroly E**,
812 **Morelli X**. 2014. Coronavirus Nsp10, a critical co-factor for activation of multiple
813 replicative enzymes. J Biol Chem **289**:25783–25796.

814 65. **Donaldson EF**, **Sims AC**, **Graham RL**, **Denison MR**, **Baric RS**. 2007. Murine hepatitis

815 virus replicase protein nsp10 is a critical regulator of viral RNA synthesis. J Virol
816 **81**:6356–6368.

817 66. **Crotty S**, **Cameron C**, **Andino R**. 2002. Ribavirin's antiviral mechanism of action: lethal
818 mutagenesis? J Mol Med **80**:86–95.

819 67. **Pathak VK**, **Temin HM**. 1992. 5-Azacytidine and RNA secondary structure increase the
820 retrovirus mutation rate. J Virol **66**:3093–3100.

821 68. **Carroll SS**, **Tomassini JE**, **Bosserman M**, **Getty K**, **Stahlhut MW**, **Eldrup AB**, **Bhat B**,
822 **Hall D**, **Simcoe AL**, **LaFemina R**, **Rutkowski CA**, **Wolanski B**, **Yang Z**, **Migliaccio G**,
823 **De Francesco R**, **Kuo LC**, **MacCoss M**, **Olsen DB**. 2003. Inhibition of hepatitis C virus
824 RNA replication by 2'-modified nucleoside analogs. J Biol Chem **278**:11979–11984.

825 69. **Lauber C**, **Goeman JJ**, **del Carmen Parquet M**, **Nga PT**, **Snijder EJ**, **Morita K**,
826 **Gorbalenya AE**. 2013. The Footprint of Genome Architecture in the Largest Genome
827 Expansion in RNA Viruses. PLoS Pathog **9**:e1003500.

828 70. **Derbyshire V**, **Grindley ND**, **Joyce CM**. 1991. The 3"-5" exonuclease of DNA
829 polymerase I of Escherichia coli: contribution of each amino acid at the active site to the
830 reaction. EMBO J **10**:17–24.

831 71. **Becares M**, **Pascual-Iglesias A**, **Nogales A**, **Sola I**, **Enjuanes L**, **Zuñiga S**. 2016.
832 Mutagenesis of Coronavirus nsp14 Reveals Its Potential Role in Modulation of the Innate
833 Immune Response. J Virol **90**:5399–5414.

834 72. **Cameron CE**, **Moustafa IM**, **Arnold JJ**. 2016. Fidelity of Nucleotide Incorporation by

the RNA-Dependent RNA Polymerase from PoliovirusDNA Replication Across Taxa, 1st ed. Elsevier Inc.

73. **Zeng J**, **Wang H**, **Xie X**, **Yang D**, **Zhou G**, **Yu L**. 2013. An increased replication fidelity mutant of foot-and-mouth disease virus retains fitness in vitro and virulence in vivo. Antiviral Res **100**:1–7.

74. **Subissi L**, **Posthuma CC**, **Collet A**, **Zevenhoven-Dobbe JC**, **Gorbalenya AE**, **Decroly E**, **Snijder EJ**, **Canard B**, **Imbert I**. 2014. One severe acute respiratory syndrome coronavirus protein complex integrates processive RNA polymerase and exonuclease activities. Proc Natl Acad Sci USA **111**:E3900–9.

75. **Imbert I**, **Guillemot J-C**, **Bourhis J-M**, **Bussetta C**, **Coutard B**, **Egloff M-P**, **Ferron F**, **Gorbalenya AE**, **Canard B**. 2006. A second, non-canonical RNA-dependent RNA polymerase in SARS coronavirus. EMBO J **25**:4933–4942.

76. **Adedeji AO**, **Marchand B**, **Velthuis te AJW**, **Snijder EJ**, **Weiss S**, **Eoff RL**, **Singh K**, **Sarafianos SG**. 2012. Mechanism of Nucleic Acid Unwinding by SARS-CoV Helicase. PLoS ONE **7**:e36521.

77. **Chaudhuri M**, **Chaudhuri M**, **Song L**, **Parris DS**. 2003. The herpes simplex virus type 1 DNA polymerase processivity factor increases fidelity without altering pre-steady-state rate constants for polymerization or excision. J Biol Chem **278**:8996–9004.

78. **Gu S**, **Li W**, **Zhang H**, **Fleming J**, **Yang W**, **Wang S**, **Wei W**, **Zhou J**, **Zhu G**, **Deng J**, **Hou J**, **Zhou Y**, **Lin S**, **Zhang X-E**, **Bi L**. 2016. The β2 clamp in the Mycobacterium tuberculosis DNA polymerase III αβ2ε replicase promotes polymerization and reduces

856 exonuclease activity. Sci Rep **6**:18418.

857 79. **Stapleford KA**, **Rozen-Gagnon K**, **Das PK**, **Saul S**, **Poirier EZ**, **Blanc H**, **Vidalain P-O**,
858 **Merits A**, **Vignuzzi M**. 2015. Viral Polymerase-Helicase Complexes Regulate
859 Replication Fidelity To Overcome Intracellular Nucleotide Depletion. J Virol **89**:11233–
860 11244.

861 80. **Agudo R**, **la Higuera de I**, **Arias A**, **Grande-Pérez A**, **Domingo E**. 2016. Involvement
862 of a joker mutation in a polymerase-independent lethal mutagenesis escape mechanism.
863 Virology **494**:257–266.

864 81. **Egloff M-P**, **Ferron F**, **Campanacci V**, **Longhi S**, **Rancurel C**, **Dutartre H**, **Snijder EJ**,
865 **Gorbalenya AE**, **Cambillau C**, **Canard B**. 2004. The severe acute respiratory syndrome-
866 coronavirus replicative protein nsp9 is a single-stranded RNA-binding subunit unique in
867 the RNA virus world. Proc Natl Acad Sci USA **101**:3792–3796.

868 82. **Bhardwaj K**, **Guarino L**, **Kao CC**. 2004. The severe acute respiratory syndrome
869 coronavirus Nsp15 protein is an endoribonuclease that prefers manganese as a cofactor. J
870 Virol **78**:12218–12224.

871 83. **Sanjuán R**, **Cuevas JM**, **Furió V**, **Holmes EC**, **Moya A**. 2007. Selection for Robustness
872 in Mutagenized RNA Viruses. PLOS Genet **3**:e93.

873 84. **Goldhill D**, **Lee A**, **Williams ESCP**, **Turner PE**. 2014. Evolvability and robustness in
874 populations of RNA virus Φ6. Frontiers in Microbiology **5**.

875 85. **Montville R**, **Froissart R**, **Remold SK**, **Tenaillon O**, **Turner PE**. 2005. Evolution of

876 mutational robustness in an RNA virus. PLoS Biol **3**:e381.

877 86. **Graci JD**, **Gnädig NF**, **Galarraga JE**, **Castro C**, **Vignuzzi M**, **Cameron CE**. 2012.
878 Mutational robustness of an RNA virus influences sensitivity to lethal mutagenesis. J
879 Virol **86**:2869–2873.

880 87. **Lauring AS**, **Acevedo A**, **Cooper SB**, **Andino R**. 2012. Codon usage determines the
881 mutational robustness, evolutionary capacity, and virulence of an RNA virus. Cell Host
882 and Microbe **12**:623–632.

883 88. **Lauring AS**, **Frydman J**, **Andino R**. 2013. The role of mutational robustness in RNA
884 virus evolution. Nat Rev Microbiol **11**:327–336.

885 89. **Aguilera ER**, **Erickson AK**, **Jesudhasan PR**, **Robinson CM**, **Pfeiffer JK**. 2017. Plaques
886 Formed by Mutagenized Viral Populations Have Elevated Coinfection Frequencies. MBio
887 **8**:e02020–16–12.

888 90. **O'Dea EB**, **Keller TE**, **Wilke CO**. 2010. Does Mutational Robustness Inhibit Extinction
889 by Lethal Mutagenesis in Viral Populations? PLoS Comput Biol **6**:e1000811–12.

890 91. **Yount B**, **Denison MR**, **Weiss SR**, **Baric RS**. 2002. Systematic assembly of a full-length
891 infectious cDNA of mouse hepatitis virus strain A59. J Virol **76**:11065–11078.

892

FIGURE 1

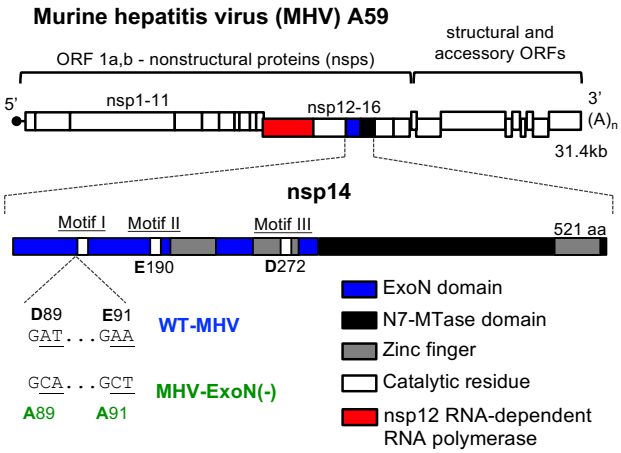

FIGURE 2

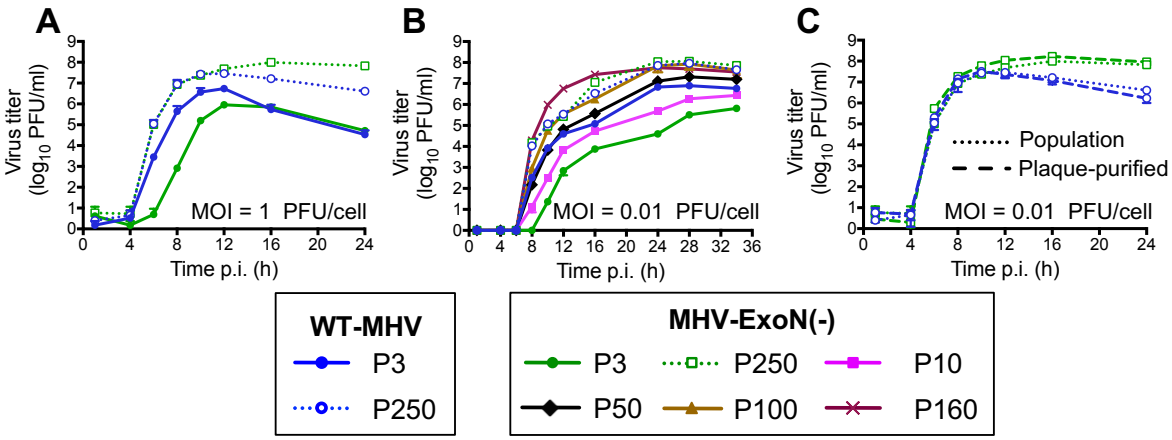

FIGURE 3

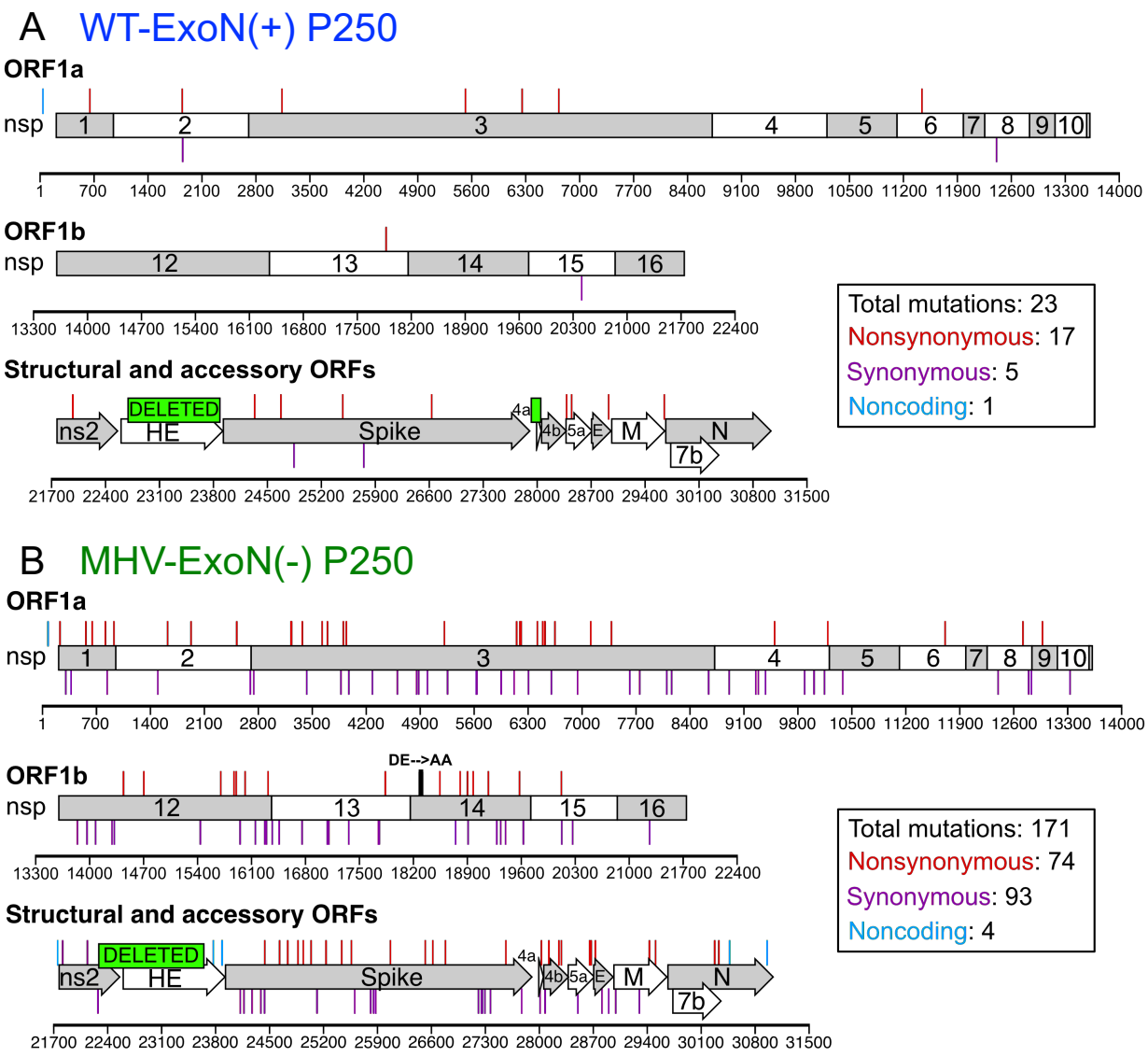

FIGURE 4

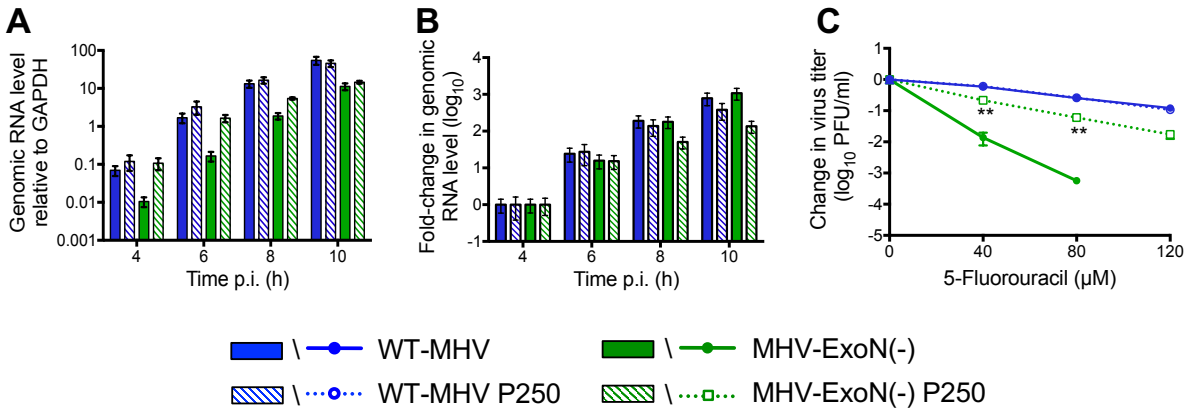

FIGURE 5

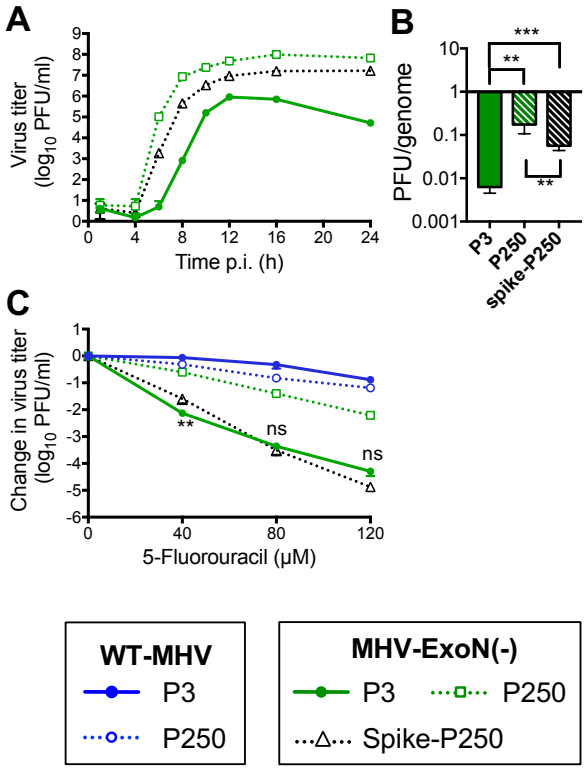

FIGURE 6

A **nsp12-RdRp:** 7 total nonsynonymous mutations

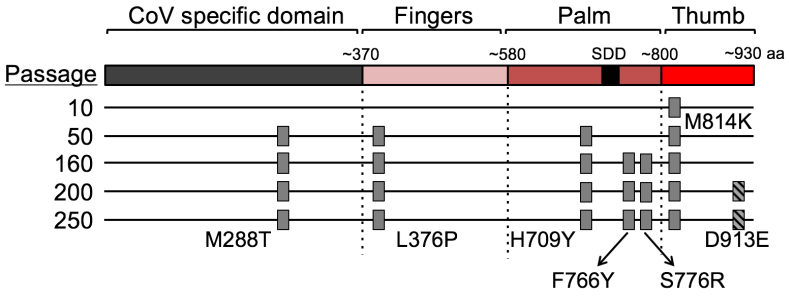

NB: No new NS changes at P31, P72, P90, P100, P120, P140, P180, P220, or P240.

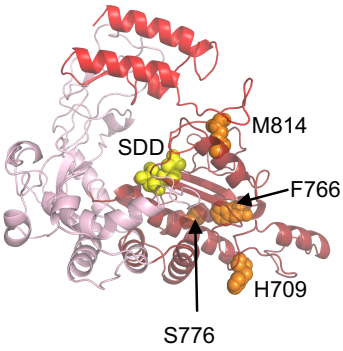

Not shown: M288, L376, D913

B **nsp14:** 6 total nonsynonymous mutations

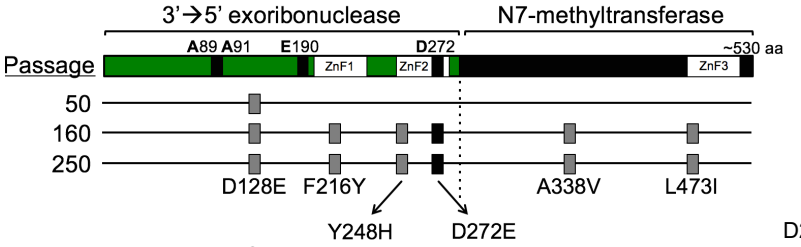

NB: No new NS changes at P10, P31, P72, P90, P100, P120, P140, P180, P200, P220, or P240.

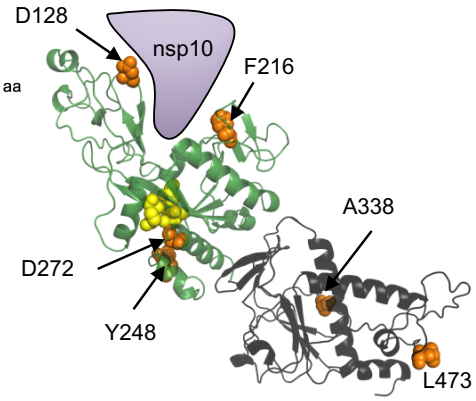

FIGURE 7

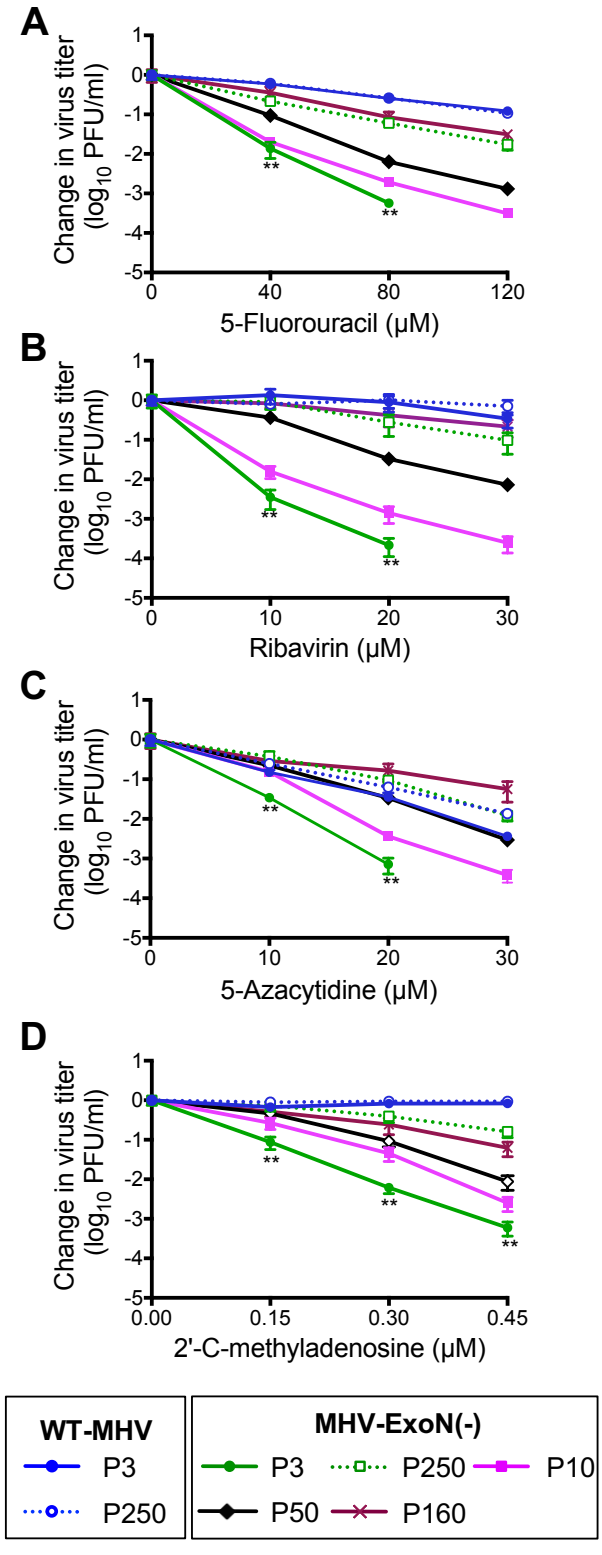

FIGURE 8